International Journal of Automotive Technology, Vol. 4, No. 4, pp. 203–211 (2003)

Article No. 1229–9138/2003/14–06

A STUDY ON IMPACT CHARACTERISTICS OF THE STACKING SEQUENCES IN CFRP COMPOSITES SUBJECTED TO FALLING-WEIGHT IMPACT LOADING

K.-H. IM[1)], N.-S. PARK[2)], Y.-N. KIM[2)] and I.-Y. YANG[2)*]

[1)]Department of Automotive Engineering, Woosuk University, Jeonbuk 565-701, Korea
[2)]School of Mechanical Engineering, Chosun University, Gwangju 501-759, Korea

(Received 8 May 2002; Revised 18 September 2003)

ABSTRACT–This paper describes a method for a falling weight impact test to estimate the impact energy absorbing characteristics and impact strength of CFRP (Carbon-fiber reinforced plastics) laminate plates based on considerations of stress wave propagation theory, which were converted to measurements of load and displacement verses time. The delamination area of impacted specimens for the different ply orientations was measured with an ultrasonic C-scanner to determine the correlation between impact energy and delamination area. The energy absorbed by a quasi-isotropic specimen having four interfaces was higher than that of orthotropic laminates with two interfaces. The more interfaces, the greater the energy absorbed. The absorbed energy of a hybrid specimen embedding GFRP (Glass-fiber reinforced plastics) layer was higher than that of normal specimens. Also, a falling weight impact tester was built to evaluate the characteristics and impact strength of CFRPs.

KEY WORDS : Composite materials, Falling weight impact test, Delamination, Impact energy and ultrasonic c-scanner

1. INTRODUCTION

Owing to the advantages associated with their very large strength-to-weight and stiffness-to-weight ratios, composite materials are attractive for a wide range of applications. Increasingly, high performance engineering structures are being built with critical structural components made from composite materials. In particular, the importance of carbon-fiber reinforced plastics (CFRP) has been generally recognized in both space and civil aircraft industries, and CFRP composite laminates are widely used. Unfortunately, CFRP laminates are too brittle under dynamic loading, particularly impact loading (Tanaka *et al.*, 1989; Advanced material committee, 1988), which can significantly reduce their properties. Therefore, the impact problems of composites have become important. A dropped wrench, bird strike (Ma *et al.*, 1991) or runway debris can generate localized delaminated areas due to foreign object damage (FOD) (Takeda, 1985), by impacts that are frequently difficult to detect with the naked eye. Although this damage may seem innocuous in the stacking plates, it can result in premature catastrophic failure due to decreased strength caused by the impact loading. For example, when a laminate is subjected to an impact load, matrix cracks and interlamina delaminations may be generated simultaneously. For this reason extensive research has been carried out, on topics such as, foreign object damage (Greszczuk, *et al.*, 1977), damage tolerance (Challenger, 1986), impact loading and residual strength (Rotem, 1988; Malvern *et al.*, 1989; Yang *et al.*, 1996), crack propagation direction in composites, and related impact damage (Mallick *et al.*, 1975; Smith *et al.*, 1987; Hong *et al.*, 1989; Young *et al.*, 1986). And failure modes have been confirmed using strength and energy concepts applied to cross-ply laminates (Garrett *et al.*, 1977; Parvizi *et al.*, 1978; Strait *et al.*, 1992). These studies derived a relationship between transverse crack spacing and laminate strain. Experimental techniques have also been offered to detect impact damage (Abrate, 1991), which focus on defining damage thresholds and considered the use of impact force as a governing parameter. In addition, temperature changes and moisture absorption have a strong bearing upon the stiffness and strength of the laminates, and the peak loading and the total absorbed energy are substantially reduced during impact when for example, a glass fiber reinforced composites is under sea water (Strait *et al.*, 1992). Thermal and thermomechanical responses of multilayered plates have been predicted and the failure of high-temperature composite structures has

*Corresponding author. e-mail: iyyang@chosun.ac.kr

also been assessed (Noor *et al.*, 1992). Also the dynamic response and damage of shell composites have been evaluated under impact (Cho *et al.*, 1999), and large deflection dynamic response of shell composites have been analyzed under impact based on nonlinear finite element analysis (Cho *et al.*, 2000).

So, impact strength evaluation has been required in order to characterize the CFRP composites. However, the strength of CFRPs under impact loading cannot be measured by the traditional standard test methods. In case of CFRPs, the standard specimen for the Charpy impact test composite has very different strengths due to its non-homogeneity, ansiotropy or the variety. Thus, it is difficult by standard testing to describe the strength of CFRPs. A falling weight impact test could be an effective way of determining the impact strength of such composites. Falling weight experiments have recently been carried out on the centers of supported composite laminates and systems are provided in order to obtain load and displacement variations during impact. However the system is not sufficiently accurate to distinguish fine differences of composite characteristics when a dynamic system is used to convert the measurements into load or deflection variations vs. time.

In this paper, a system to obtain load and deflection variations in time at applied impact points has been developed for a falling impact type on composites fixed by circular frames. Also a circular bar with added mass was used as a falling weight, and strain variations in time at two different points of the bar were measured to convert the measurements to load and displacements using one dimensional wave theory.

This system has been applied to evaluate the impact energy absorbtion of CFRP composite laminates with various stacking sequences and for hybrid specimens containing a GFRP layer. In addition, a ultrasonic C-scanner was utilized to find the correlation between impact energy and delamination area under falling weight impact.

2. THEORY

A measuring system using strain gauges was developed, which provides responses to impact loads and deflections of specimens with considerable accuracy. A falling weight impact test, such as a circular bar with added mass, which strikes the specimen with a velocity Vo was considered, as shown in Figure 1. Two sets of strain gauges are affixed at distances L1 and L2 from the lower impact end of the bar. The impact load actually acting on the specimen and even the deflection at the impact-induced point can be derived from the measurements of strains using one-dimensional theory of elasticity.

The theoretical background demonstrates how the load

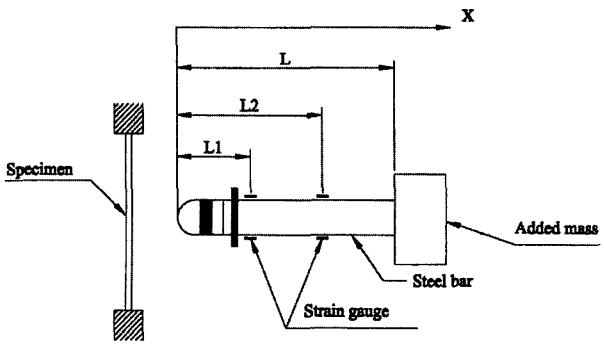

Figure 1. Drop-weight and coordinates.

and deflection variations in time can be obtained at the impact point from the measured strain variations in time at two different points on the bar. In Figure 1, L is the length, A is the cross-sectional area of falling weight bar, E is Youngs' modulus and ρ is the density of the bar. It is assumed that the waves propagated in the bar are governed by the following one-dimensional theory (Adachi *et al.*, 1986).

$$\frac{\partial^2 u}{\partial x^2} = \frac{1}{c^2}\frac{\partial^2 u}{\partial t^2} \tag{1}$$

$$\text{where } C = \sqrt{\frac{E}{\rho}} \tag{2}$$

where x, u, t and C are the coordinate, displacement, time and propagating velocity of the waves, respectively. The Laplace transformation is introduced to solve Equation (1). Initial conditions are given as follows:

$$\left.\frac{\partial u}{\partial t}\right|_{t=0} = -v_0 \tag{3}$$

Then, the Laplace transformation of Equation (1) is obtained by the equation.

$$\int_0^\infty \frac{\partial^2 u}{\partial x^2} e^{-st} dt = \frac{v_0}{C^2} + \frac{S^2}{C^2} U_{(s)} \tag{4}$$

where s is Laplace transformation operator.

Ordinary differential equations are obtained from Equation (1) below.

$$\frac{d^2 U_{(s)}}{dx^2} - \frac{S^2}{C^2} U_{(s)} = \frac{v_0}{C^2} \tag{5}$$

here $U = \int_0^\infty u e^{-st} dt$, and the general solution of Equation (5) is:

$$U_{(s)} = A_1 e^{\frac{Sx}{C}} + A_2 e^{\frac{Sx}{C}} - \frac{v_0}{s^2} \tag{6}$$

Boundary conditions at both ends of the bar are

required to determine the coefficients A_1 and A_2. However, in this problem the boundary conditions cannot be defined and are unknown.

$$\frac{\partial U}{\partial x} = \frac{S}{c}\left\{A_1 e^{\frac{Sx}{c}} - A_2 e^{\frac{Sx}{c}}\right\} \tag{7}$$

Boundary conditions of the bar should be solved in inverse order using the strain responses at two different points of the bar, which are obtained by measurements. Now suppose the strain variations in time are known such that:

$$x = l_1: \frac{\partial U}{\partial x} = \varepsilon_1(t)$$
$$x = l_2: \frac{\partial U}{\partial x} = \varepsilon_2(t) \tag{8}$$

The Laplace transformations of Equation (8) are:

$$x = l_1: \frac{\partial U_{(s)}}{\partial x} = \bar{\varepsilon}_1(s)$$
$$x = l_2: \frac{\partial U_{(s)}}{\partial x} = \bar{\varepsilon}_2(s) \tag{9}$$

Therefore Equation (7), when x is l_1, l_2 yields:

$$\bar{\varepsilon}_1 = \frac{S}{C}A_1 e^{\frac{sl_1}{c}} - \frac{S}{S}A_2 e^{\frac{sl_1}{c}}$$
$$\bar{\varepsilon}_2 = \frac{S}{C}A_1 e^{\frac{sl_2}{c}} - \frac{S}{S}A_2 e^{\frac{sl_2}{c}} \tag{10}$$

Solving Equation (10), the coefficients A_1, A_2 may be determined using:

$$A_1 = \frac{C}{S}\frac{-\bar{\varepsilon}_1 e^{(-sl_2/c)} + \bar{\varepsilon}_2 e^{(-\varepsilon l_1/c)}}{2\sinh\{s(l_2 - l_1)/c\}}$$
$$A_2 = \frac{C}{S}\frac{-\bar{\varepsilon}_1 e^{(-sl_2/c)} + \bar{\varepsilon}_2 e^{(-\varepsilon l_1/c)}}{2\sinh\{s(l_2 - l_1)/c\}} \tag{11}$$

The load F and the deflection w of the impact point i.e. the distance between the contact point and the end of the impact bar can be expressed by a Laplace transformation as follows:

$$F(t) = -AE\varepsilon|_{x=0}$$
$$W(t) = -(u)_{x=0} \tag{12}$$

The Laplace transformations of Equation (11) are.

$$\bar{F}(s) = -AE\bar{\varepsilon}|_{x=0}$$
$$\bar{W}(s) = -(u)_{x=0} \tag{13}$$

Thus, using Equations (6), (7) and (11), Equation (13) may be expressed as:

$$\bar{F}(s) = AE\frac{-\bar{\varepsilon}_1\sinh(sl_2/c) + -\bar{\varepsilon}_2\sinh(sl_1/c)}{\sinh\{s(l_2 - l_1)/c\}}$$
$$\bar{W}(s) = \frac{c}{s}\frac{\bar{\varepsilon}_1\cosh(sl_2/c) - \bar{\varepsilon}_2\cosh(sl_1/c)}{\sinh\{s(l_2 - l_1)/c\}} + \frac{v_0}{s^2} \tag{14}$$

Using the Laplace transformation of Equation (14), the loading and displacement variations in time are obtained. The resulting problem is how to get the Laplace inverse transformation of Equation (14). The analytical procedure is as follows. From Equation (14), it seems like that the solution for the load F can be obtained analytically. In the case of l_1=l/3, l_2=2l/3 the load F has the following form.

$$\bar{F}(s) = [-\bar{\varepsilon}_1\{e^{(sl/3c)} + e^{(-sl/3c)}\} + \bar{\varepsilon}_2]AE \tag{15}$$

Using the shifting theorem the Laplace transformation of Equation (15) is readily derived as: (Moligoch *et al.*, 1988)

$$F(t) = -AE\{(t + l/3c)H(t + l/3c) +$$
$$\varepsilon_1(t - l/3c)H(t - l/3c) - \varepsilon_2(t)H(t)\} \tag{16}$$

Using the shifting theorem the Laplace transformation of Equation (15) is readily derived in the case of no added mass when $l_1 = l/2$, $l_2 = l$, $\varepsilon_2(t) = 0$ at x=l/2, as follows:

$$F(t) = -AE\{\varepsilon_1(t + l/3c)H(t + l/3c) +$$
$$+ \varepsilon_1(t - l/3c)H\} \tag{17}$$

Where $H(t)$ is the Heaveiside unit step function.

Then substituting the measured strain variations in time, $\varepsilon_1(t)$ and $\varepsilon_2(t)$, into Equation (17), the force variations in time are obtained. However, the solution for the deflection W in Equation (14) can only be obtained as an infinite series. On the other hand, a powerful numerical method is as follows. First, $\varepsilon_1(p)$ and $\varepsilon_2(p)$ are numerically given by the discrete Laplace transformation for the experimental data, $\varepsilon_1(t)$ and $\varepsilon_2(t)$ are sampled discretely from the strain variations in time. Next, substituting these discrete values of $\varepsilon_1(p)$ and $\varepsilon_2(p)$ into Equation (14), the Laplace inverse transformations of the discrete values of $F(p)$ and $W(p)$ are obtained numerically. Also an accurate value for the velocity is needed. This procedure requires a lot of data to be handled properly, but an FFT algorithm can be used to significantly reduce the computing time.

The Laplace and inverse Laplace tranmation equations are shown in Equation (18). Here, s is the Laplace transformation parameter. If Equation (18) is applied to change of variable change by $s = \gamma + iw$, a form of line integral and to complex line integral, Equation (19) could be expressed as follows:

$$\bar{F}(s) = \int_0^\infty F(t)e^{(-st)}dt$$

$$F(t) = \frac{1}{2\pi}\int_{\gamma-i\infty}^{\gamma+i\infty} \bar{F}(\gamma+iw)e^{\{t(\gamma-iw)\}/i}dw \quad (18)$$

$$F(t) = \frac{1}{2\pi}\int_{\gamma-i\infty}^{\gamma+i\infty} \bar{F}(\gamma+iw)e^{\{t(\gamma-iw)\}/i}dw$$

$$= e^{(\gamma t)}\frac{1}{2\pi}\int_{-\infty}^{\infty} \bar{F}(\gamma+iw)e^{(iwt)}dw \quad (19)$$

Here, $w = n\Delta w$, and $t = k\Delta t$, Equation (20) can be obtained by using a discrete distribution as follows;

$$F(k\Delta) = \frac{\Delta w t^{(\gamma k\Delta t)}}{2\pi}\sum_{-\infty}^{\infty} \bar{F}(\gamma+in\Delta w)e^{(in\Delta wk\Delta t)}$$

$$k = 1, 2, 3, \ldots, \infty \quad (20)$$

Here, a discrete width is as follow using a sampling principle. $\Delta w = 2\pi/T$, $\Delta t = T/N$ where ϖ is the sampling. $F(t)$ range is obtained within $0 \le t \le T$ and the range of $F(g + iw)$ is within $0 \le w \le w_{max}$ because $2\pi/\Delta w$ represents the time limit. The Laplace and inverse Laplace transformation equations are obtained by discrete Fourier transformation as follows:

$$F(\gamma+in\Delta w) = \Delta t\sum_{r=0}^{N-1} [F(k\Delta)e^{(-\gamma k\Delta t)}]e^{\{-i(2\pi/N)nk\}}$$

$$F(k\Delta t) = \frac{e^{(\gamma k\Delta t)N-1}}{T}\sum_{n=0} [\bar{F}(\gamma+in\Delta w)]e^{\{i(2\pi/N)nk\}} \quad (21)$$

In this paper the experimental and analytical methods are employed for the load and the deflection, respectively. These steps can derive the impact load and deflection of the specimen variations in time at impact point. The background is based entirely on the assumption that the one-dimensional theory of wave propagation expressed by the Equation (1) is effective. The verification of measuring system developed is presented in a paper (Im *et al.*, 2000).

3. EXPERIMENTAL METHOD

3.1. Specimen Configurations

The laminate specimens were manufactured from one-directional prepreg sheets of CU125NS carbon fibers which fibers are consisted with no scrim in Hankook Fiber (Hankook Fiber Composites, 2001), cured to the manufacturer's specifications. Four types of specimens were used, as follows: specimen A $[0°_4/90°_4]$s, B $[0°_2/45°_2/90°_2/-45°_2]$s, C $[0°_2/90°_2/0°_2]$s and D $[0°_2/90°_7(\theta_2)/0°_4]$. Test specimens were prepared with dimensions 200 mm × 200 mm × 2.5 mm (width × length × thickness), and the fiber-direction of specimen surface was manufactured to correspond to 0° direction. Thus, the fiber-direction lies along the length. By properly manipulating the harding temperature point using an autoclave, the CFRP laminates can be cured. After laminating the prepregs in the desired direction, the inner temperature was heated up to 125°C. After keeping the vacuuming condition of the vacuum bag up to 10^{-1} Pa in forming. the pressure of 5×10^5 Pa was added to the vacuum bag from the outer side of the bag by using the compressor.

3.2. Falling Weight Impact Experimentation

The system developed during this is shown in Figure 2 and Figure 3 shows schematic dimensions of falling weight. The impactor masses were 0.58 kg (falling weight I) and 0.84 kg (a falling weight II) and dimension is 600 mm in length and 10 mm in diameter. The curvature of the impactor end was 14 mm. Specimens were clamped by two pieces of circular frames of 150 mm in diameter before testing and the falling weight strikes the center of the specimens. The strain gauge based method was employed as a measuring system. Also

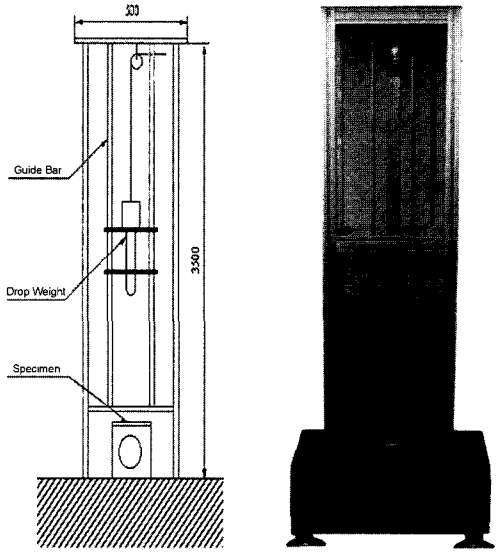

Figure 2. Schematic diagram of falling weight tester.

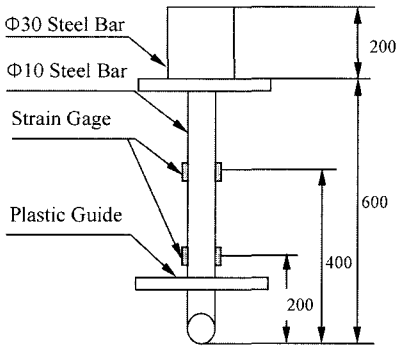

Figure 3. Schematic diagram of falling weight.

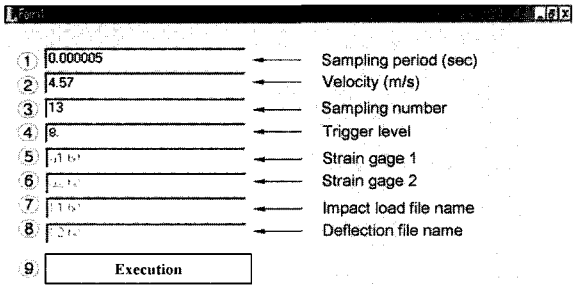

Figure 4. Screen capture of soft program.

the optical displacement transducer was used to measure displacement of the specimens after impact. The velocity of the falling weight impactor was measured just before impact by determining the time taken for it to pass two fine laser beams located a known distance apart. The impact energy was about 3.78J (at a velocity of 3.0 m/s) and 12.71J (with a velocity of 5.5 m/s). The impact energy (J) shown is the kinetic energy of the impactor prior to impact. Figure 4 shows a screen capture of home-made soft program. After impacting testing, data from strain gage and optical displacement transducers have been obtained and then impact load and deflection could be easily solved using the program based on theory. Here strain variations in time $\varepsilon_1(t)$, $\varepsilon_2(t)$ directly from the measured raw data are shown in Figure 1, where the responses are observed because of the propagation of the

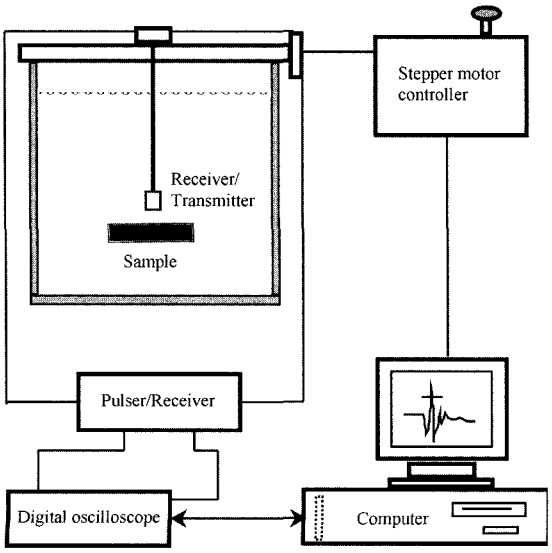

Figure 5. Experimental setup for pulse-echo scan mode in immersion tank.

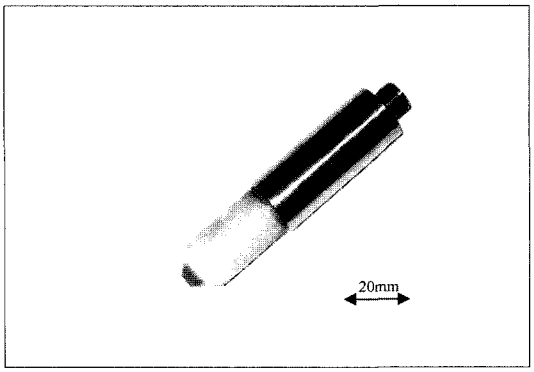

Figure 6. Transducer used in this test.

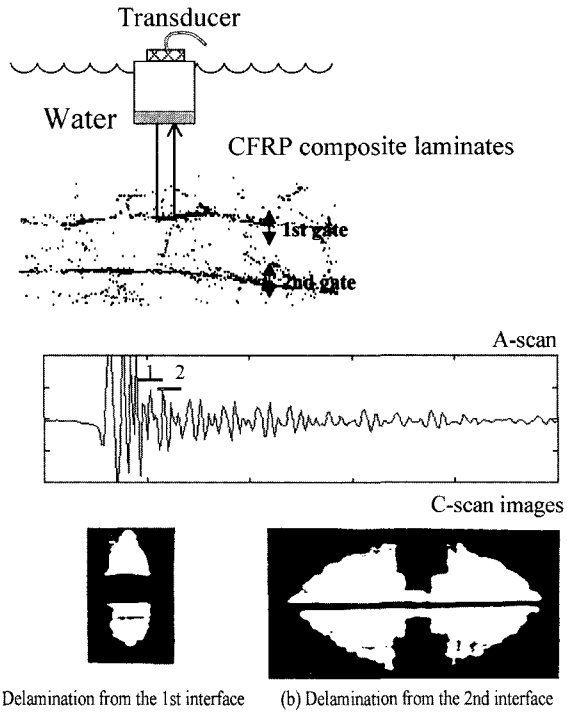

Figure 7. Inspection method of composite laminated damages using ultrasonic C-scanner.

elastic waves along the impactor. Also the load and the deflection variations in time are obtained through data processing based on Equation (14).

3.3. Damage Detection Techniques

Pulse echo ultrasonic C-scans wconducted in an immersion tank using a Sonix scanning system. 50 MHz, 6.35 mm diameter, focused transducers were aligned perpendicular to the disk and driven by a Panametrics 5052 pulser/receiver. Figure 5 shows an experimental setup for pulse-echo scan mode in immersion tank. The measuring

methods for the delamination areas were as follows; each interface was classified by color, the distributed range of each color was measured using an ultrasonic C-scanner, and the total delamination area was obtained by summing the delamination areas. Figure 6 shows a transducer used in this test. Figure 7 shows a method to inspect impact damages of CFRP composite laminates using ultrasonic C-scanner. After impact, the delamination of the specimen interfaces was assessed using a pulse-echo ultrasonic C-scan. In terms of the principle of ultrasonic C-scanner, the amplitude and time-of-flight of the (first arrival) transmitted pulse are used to generate the amplitude and time-of-flight images. The pulse echo measurement samples the integrated material properties across the thickness.

4. EXPERIMENTAL RESULTS AND DISCUSSION

4.1. Static Experimentation

CFRP composite laminates were supported by a fixture and compressive testing was carried out using a circular bar, with 14 mm curvature, on a universal testing machine. The relationship between loading and displacement was obtained until the failure. Table 1 shows the results of the static testing under the same conditions as the impact tests.

4.2. Impact Experimentation

When a falling weight impacted on the CFRP composite laminates, characteristics of the loading, displacement and absorbed energy were considered verse the stacking sequences of the CFRP laminates. Figure 8 shows the load-time curve and the load-displacement curve of the orthotropic specimen A with 2 interfaces using weight II (added mass). In the Figure 8, oscillations such as noises in the curve line were observed due to the fiber failure upon impact. The load and displacement relationship is probably one of the most important. In this section the dynamic load and displacement relationship during falling measurement by eliminating time between the load and the displacement variations in time. The area enclosed by loading and unloading can be considered as energy absorbed consumed by the specimen fracture, as shown in Figure 7(b).

4.3. Impact Damages and Observation of Inner-Damaged Development

Table 1. Results of static test.

Specimens type	A	B	C	D
Maximum load Fmax [kN]	2.92	3.04	4.34	4.04

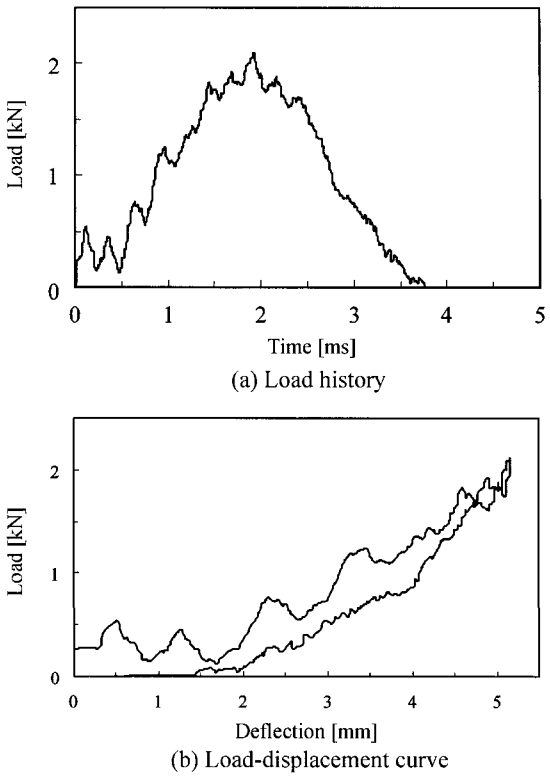

Figure 8. Falling-weight test of CL2 (Impact energy: 5.74J).

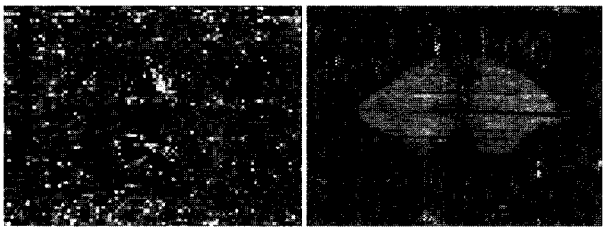

Figure 9. Typical delamination shapes of specimens (a) $[0^\circ_4/90^\circ_4]$s and (b) $[0^\circ_4/90^\circ_7(\theta_1)/0^\circ_4]$ on the rear side of impact point.

To estimate the impact-induced damage area the C-scanning was conducted in an immersion tank in order to reduce attenuation, scattering and absorption during impact. Figure 9 shows typical delamination shapes of specimen [0/90] and [0/90(θ)/0]. In case of a specimen with two interfaces, the damaged area was easily measured; however, in case of a specimen with four interfaces, damaged area was not easily measured. Therefore, the area was measured as the projected area due to the characteristics of the C-scanner.

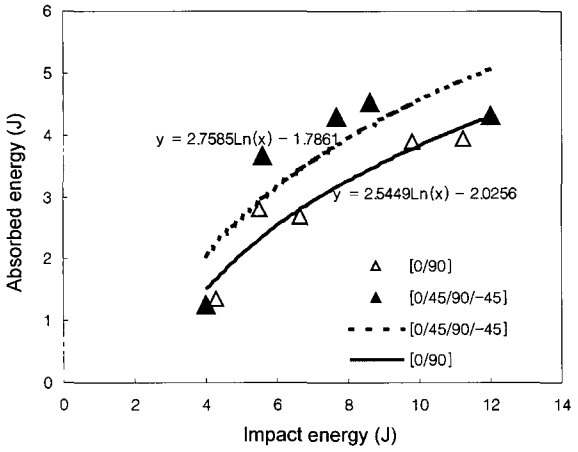

Figure 10. Relation between absorbed energy and impact energy (specimen [0/90] A, specimen [0/45/90/-45] B).

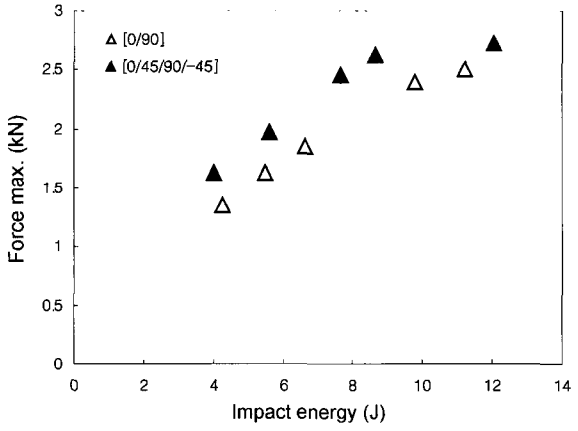

Figure 11. Relation between maximum load and impact energy (specimen [0/90] A, specimen [0/45/90/-45] B).

4.4. Effects of Stacking Sequences

Figure 10 shows the relation between the absorbed energy and the impact energy for specimens A and B with the same stacking number and different stacking sequences and curve fitting equations also. In the Figure 9, the symbol (△) means orthotropic laminate [0/90] specimen A with 2 interfaces and the symbol (▲) is a quasi-isotropic laminate [0/45/90/-45] specimen B with 6 interfaces. The energy absorbed by specimen A is almost the same as that of specimen B at an impact energy of about 4J. However the absorbed energy of the quasi-isotropic specimen B is higher than that of orthotropic specimen A as the impact energy increases. It is believed that the interface number and stacking sequences increased the energy absorbed. Figure 11 shows the relation between the maximum load and the impact energy for the specimen A [0/90] and specimen B [0/45/90/-45]. Impact energies of each specimen increase as the impact energy becomes greater.

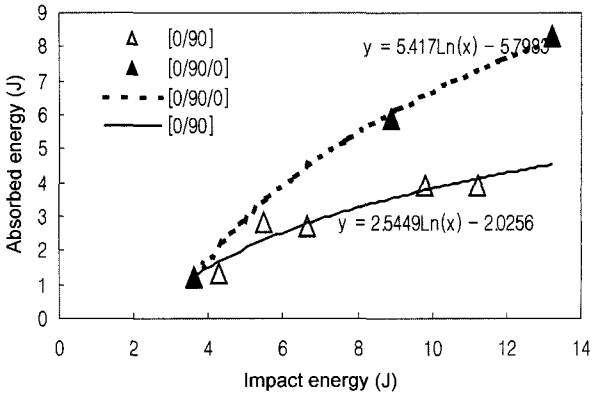

Figure 12. Relation between absorbed energy and impact energy (specimen [0/90] A, specimen [0/90/0] C).

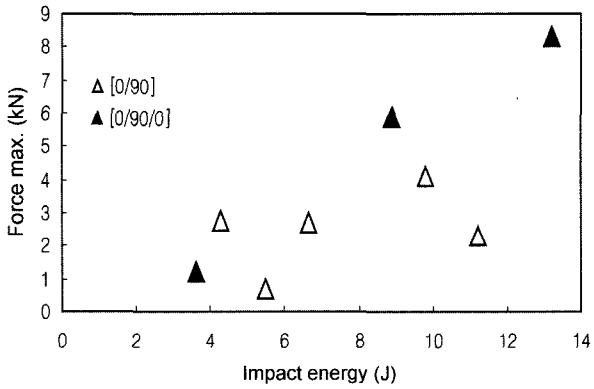

Figure 13. Relation between maximum load and impact energy (specimen [0/90] A, specimen [0/90/0] C).

Figure 12 shows the relation between the absorbed energy and the impact energy for specimens [0/90] A and [0/90/0] C and curve fitting equations also. The interfaces of the specimen [0/90] A and specimen [0/90/0] C are 2 and 4 respectively, and all were orthotropic laminates. Figure 12. does not show any difference between absorbed energy and impact energy at around an impact energy of 4J. As the impact energy is increased, the absorbed energy of specimen C becomes higher than that of specimen A. This greater absorbed energy were attributed to the higher interface numbers of specimen C with much more interface number. Figure 13 shows the relation between the maximum load and impact energy for the specimens A and C. Force maximum loads of specimens A and C are almost similar to some degree.

Hybrid means mixture of two more fibers. Here, carbon and a glass fiber mixes were evaluated using the falling weight impact test equipment. Figure 14 shows

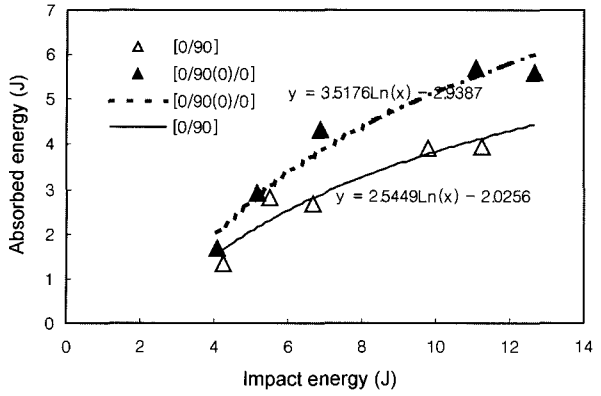

Figure 14. Relation between absorbed energy and impact energy (specimen [0/90] A, specimen [0/90(0)/0] D).

the relation between absorbed energy and impact energy for specimen [0/90] A and specimen [0/90(θ)/0] D, the center of which contained a GFRP layer at its θ interface and curve fitting equations also. Here the means a glass fiber. Generally, the absorbed energy of specimen D with GFRP layer was greater than that of specimen A as the impact energy increased. So it is believed that a inserting the foreign bending stiffness of a a hybrid made the specimen absorb more energy because of the greater delamination of the specimen interfaces.

4.5. Relationship Between Stacking Sequences and Impact Damage Area

Figure 15 shows the relation between impact energy and delamiantion area of specimen [0/90] A and specimen [0/45/90/-45] B with the same interface number and different stacking sequences. The relation between impact energy and delamination area was linear for both specimens. Also, it was believed that the critical delamination impact

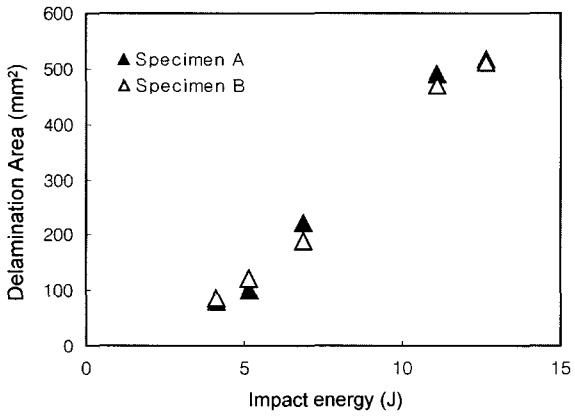

Figure 15. Relation between impact energy and delamination area of specimens A and B.

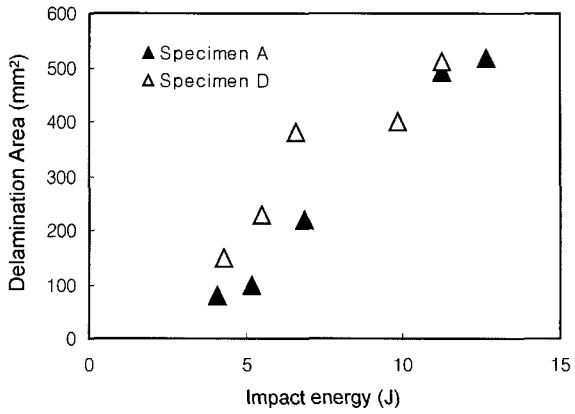

Figure 16. Relation between impact energy and delamination area of specimens A and D.

energies are about 2.61J and 2.53J for specimens A and B, respectively. Thus, it is determined that the relation between impact energy and delamination area was similar for specimens A and B. Figure 16 shows the relation between the impact energy and the delamination area of specimens [0/90] A and [0/90(θ)/0] D, containing hybrid layer. A linear relation was observed for the specimen A and D. In addition the critical delamination impact energies of specimens A and D were approximately 3.21J and 2.01J, respectively. Even if specimens have the same interface number and stacking sequence, the delamination area of specimen D was higher than that of specimen A; but the critical delamination impact energy of specimen D was lower than that of specimen A. Thus it is believed that the hybrid fiber was partly fractured and that the fiber absorbed much more energy during impact.

5. CONCLUSIONS

In this paper, a developed falling weight impact tester is described, and used to estimate the absorbing characteristics. After impacting CFRP laminates of various interface number and stacking sequences, the delaminated areas were observed using an ultrasonic C-scanner and the correlation between impact energy and delamination area determined.

The following conclusions can be drawn from our results:

(1) An assessment system using a falling weight impactor has been developed on the basis of stress wave propagation considerations.

(2) It was found that the absorbing energy of quasi-isotropic CFRP laminates is greater than that of orthotropic laminates, but that the relation between impact energy and delamination area is almost the

same for the specimens A and B.

(3) The energy absorbed CFRP laminates with four interfaces is much greater than that of CFRP laminates with two interfaces which were all constructed with the same stacking number and matrix; it is believed that the greater the number of interfaces the more energy will be absorbed at impact.

(4) In case of the same stacking number and stacking sequences, hybrid specimens containing a GFRP layer was greater than that of normal specimens.

(5) In case of the same interface number and stacking sequences, the delamination area of specimen D was found to be higher than that of specimen A; however the critical delamination impact energy of specimen D was lower than that of specimen A. Thus, it is believed that specimens with hybrid fiber are partly fractured and that the fiber absorbs much more energy during impact.

REFERENCES

Abrate, S. (1991). Impact on laminated composite materials. *Appl. Mech. Rev.* **44, 4,** 155–190.

Adachi, T., Ujihashi, S. and Matsumoto, H. (1986). Impulsive response to a finite circular cylindrical shell subjected to waterhammer waves. *Bulletin of JSME* **29, 249,** 737–742.

Advanced material committee: *Advanced Materials and Book.* (1988). HwanSun in Japan No.45, Tokyo.

Challenger, K. D. (1986). The damage tolerance of carbon fiber reinforced composites-A workshop summary. *Composite Struct.*, 295–318.

Cho, C. D. and Zhao, G. P. (1999). Dynamic response and damage of composite shell under impact. *KSME Int. J.* **13, 9,** 596–608.

Cho, C. D., Zhao, G. and Kim, C. B. (2000). Nonlinear finite element analysis of composite shell under impact. *KSME Int. J.* **14, 6,** 666–674.

Garrett, K. W. and Bailey, J. E. (1997). Multiple transverse failure in 90 degree cross-ply laminate of a glass fiber-reinforced polyester. *J. Mat. Sci.* **12,** 157–168.

Greszczuk, L. B. and Chao, H. (1977). *Impact Damage in Graphite-Fiber-Reinforced Composites.* ASTM STP 617, ASTM. Philadelphia, 389–408.

Hankook Fiber Composites (2001). Was Provided by Hankook Fiber Co. Milyang, Korea.

Hong, S. (1989). On the relationship between impact energy and delamination area. *Experimental Mechanics* **29, 2,** 115–120.

Im, K. H., Park, N. S. and Yang, I. Y. (2000). A Study on the influence of stacking sequences using CFRP laminates plates by falling weight impact. *The Korean Proceeding for Composite Materials* **1, 1,** 106–109.

Ishai, O. and Shragi, A. (1990). Effect of impact loading on damage and residual compressive strength of CFRP laminated beams. *Composite Struct.* **14, 4,** 319–337.

Strait, L. H., Karasek, M. L. and Amateau, M. F. (1992). Effects of stacking sequence on the impact resistance of carbon fiber reinforced thermoplastic toughened epoxy composite. *J. of Composite Materials* **26, 12,** 1725–1740.

Ma, C. C. M., Huang, Y. H. and Chang, M. J. (1991). Hygrothermal effect on the PEEK/C.F. and PPS/C. F. under impact loading(I). *ANTEC,* 2029–2096.

Malvern, L. E., Sun, C. T. and Liu, D. (1989). Delamination damage in central impacts at subperformation speeds on laminated kevlar/epoxy plates. *ASTM. STP.* **1012,** 387–405.

Miller, A. K. and Adams, D. F. (1975). An analysis of the impact behavior of hybrid composite materials. *Material Science and Engineering* **19,** 245–260.

Moligoch, C. E., Wooda, C. H. and Hedochi, C. (1988). *Mathematics Equations,* Armpa **1, 1,** 66–163. Tokyo.

Noor, A. K. and Burton, U. S. (1992). Computational models for high-temperature multilayered composite plates and shells. *Appl. Mech Revc.* **45, 10,** 419–446.

Parvizi, A. and Bailey, J. E. (1978). On multiple transverse cracking in glass fiber expoxy cross-ply laminates. *J. Mat. Sci.* **13,** 2131–2136.

Rotem, A. (1988). Residual flexural strength of FRP composite specimens subjected to transverse impact loading. *SAMPE Journal,* 19–25.

Strait, L. H., Karasek, M. L. and Amateau, M. F. (1992). Effects of sea water immersion on the impact resistance of glass reinforced epoxy composites. *J. Composite Mat.* **26, 12,** 1725–1740.

Tanaka, T. and Kurokawa, T. (1989). Damage and residual bending strength of graphite/epoxy composite laminates subjected to normal impact. *J. of the Japan Society for Aeronautical & Space Sciences* **37, 25,** 29–36.

Takeda, T. (1985). Impulsive response and fracture of composites (I). *J. of the Japan Society for Composite Materials* **11, 4,** 151–161.

Yang, I. Y., Sim, J. K. and Im, K. H. (1996). Impact damages and residual bending strength of CFRP composite laminates subjected to impact loading. *KSME Int. J.* **10, 4,** 423–434.

Young, D. and Sung, B. (1986). Horizontal wing structure of civil airplane using composite materials. *J. of the Japan Society for Aeronautical and Space Science* **34, 394,** 608–618.